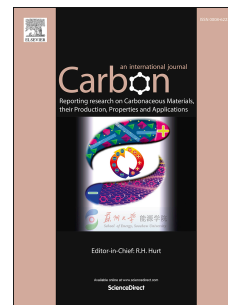


Journal Pre-proof

Regulation of interface between carbon nanotubes-aluminum and its strengthening effect in CNTs reinforced aluminum matrix nanocomposites

Xin Zhang, Shufeng Li, Bo Pan, Deng Pan, Lei Liu, Xiaodong Hou, Mingqiang Chu, Katsuyoshi Kondoh, Maiqun Zhao



PII: S0008-6223(19)30915-7

DOI: <https://doi.org/10.1016/j.carbon.2019.09.016>

Reference: CARBON 14586

To appear in: *Carbon*

Received Date: 13 May 2019

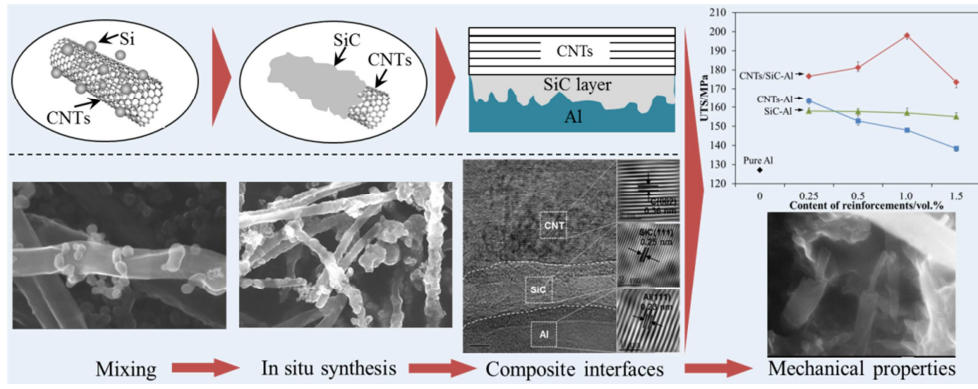
Revised Date: 16 July 2019

Accepted Date: 4 September 2019

Please cite this article as: X. Zhang, S. Li, B. Pan, D. Pan, L. Liu, X. Hou, M. Chu, K. Kondoh, M. Zhao, Regulation of interface between carbon nanotubes-aluminum and its strengthening effect in CNTs reinforced aluminum matrix nanocomposites, *Carbon* (2019), doi: <https://doi.org/10.1016/j.carbon.2019.09.016>.

This is a PDF file of an article that has undergone enhancements after acceptance, such as the addition of a cover page and metadata, and formatting for readability, but it is not yet the definitive version of record. This version will undergo additional copyediting, typesetting and review before it is published in its final form, but we are providing this version to give early visibility of the article. Please note that, during the production process, errors may be discovered which could affect the content, and all legal disclaimers that apply to the journal pertain.

© 2019 Published by Elsevier Ltd.



Journal Pre-proof

Regulation of interface between carbon nanotubes-aluminum and its strengthening effect in CNTs reinforced aluminum matrix nanocomposites

Xin Zhang ^a, Shufeng Li ^{a,*}, Bo Pan ^{b,*}, Deng Pan ^a, Lei Liu ^a, Xiaodong Hou ^c, Mingqiang Chu ^d, Katsuyoshi Kondoh ^e, Maiqun Zhao ^a

^a *School of Materials Science and Engineering, Xi'an University of Technology, NO.5 South Jinhua Road, Xi'an, 710048, China*

^b *Xi'an Thermal Power Research Institute Co. Ltd., No.99 Yanxiang Road, Xi'an, 710054, China*

^c *Research Institute for Future Transport & Cities, Coventry University, Coventry, Priory Street, Coventry, CV1 5FB, United Kingdom*

^d *Shanghai Aircraft Manufacturing Co, Ltd., 919 Shangfei Road, Shanghai, 200436, China*

^e *Joining and Welding Research Institution, Osaka University, 11-1 Mihogaoka, Ibaraki, Osaka, 567-0047, Japan*

**Corresponding author: E-mail: shufengli@xaut.edu.cn (S. Li); panbo@tpri.com.cn (B. Pan)*

Abstract

Carbon nanotubes (CNTs) are popular as the chosen reinforcement to achieve excellent mechanical and functional performance in aluminum matrix nanocomposites (AMNCs). However, the key bottleneck problems restrict the strengthening effect using CNTs in AMNCs due to the dispersion homogeneity of CNTs, the distinct differences in physical properties, poor wettability and interface bonding between CNTs and aluminum matrix. This study aims to address these key issues by introducing a continuous SiC nano layer synthesized from carbon-silicon reaction, acting as a compatibility transition layer prior to mixing with aluminum powders. The results clearly show that the SiC cladding layer provides a good wettability and strong interfacial bonding between CNTs and aluminum matrix, and the interfacial reaction between

CNTs and aluminum matrix could be effectively regulated. It is also conducive to reducing the mass density difference and specific surface energy, improving the dispersion of CNTs in matrix. Those factors make a strong contribution to the strengthening effect of CNTs enforcement by achieving high load transfer efficiency. The AMNCs reinforced by this new CNTs/SiC composite powder show clear improvement of mechanical performance without compromising in ductility and electrical conductivity, as compared to AMNCs reinforced by only CNTs or SiC.

1. Introduction

Lightweight materials offer great advantages to tackle the energy crisis and environmental pollution by reducing the component weight but maintaining the strength. Among these lightweight materials, Al based nanocomposite have been extensively studied due to its great potential for good mechanical performance with relatively low cost [1-4]. Carbon nanotubes (CNTs) have shown excellent mechanical and functional characteristics such as extreme high strength, ultrahigh Young's modulus, thermal and electrical properties, hence considered as an ideal reinforcing phase for composite materials [5, 6]. Actually, CNTs reinforced aluminum matrix nanocomposites (AMNCs) have already attracted wide attention because it offers a rout to achieve both excellent structural and functional properties, including low density, higher specific strength, low expansion coefficient, excellent thermal and electrical conductivity [7-10]. AMNCs show broad application prospects in the fields of aerospace, automotive and transportation, meeting the increasing demand for high-performance materials in engine parts, high-speed train brake system and a wide range of other key industrial components [11, 12].

Great efforts have been made to improve the properties of AMNCs by utilizing the super-high strength and good conductivity of CNTs as an enforcement. In particular, significant progress has been made in improving their mechanical performance [13-15]. It was reported that

the tensile strengths of CNTs reinforced AMNCs were effectively improved (to be over 200 MPa), but the high strength was achieved at the expense of ductility (reduce to less than 6%) and other functional properties [9, 16]. The performance of AMNCs strongly depends on the distribution of CNTs in Al matrix, but the mass density difference makes CNTs difficult to disperse uniformly [17-19]. CNTs tend to agglomerate due to the large Van der Waals force which caused by its small size, and lead to poor compatibility in metals. The agglomeration trend of CNTs is associated with specific surface energy, surface tension and the characteristics of the complex interface bonding and the wettability between CNTs and Al matrix [20, 21]. Among these factors, the poor wettability needs be addressed primarily, due to the distinct differences in physical properties between CNTs and Al [22-24]. In previous studies, it was suggested that introducing an Al_4C_3 interlayer via reaction between CNTs-Al could improve the wettability between CNTs and Al matrix, but this interlayer should be well designed and elaborated. Interface layer without carefully optimization could easily cause Al_4C_3 unstable and hydrolyzed: superabundant Al_4C_3 formed in AMNCs will compromise the mechanical performance by causing severe failure during service [25-27]. In summary, poor wettability, homogeneity, interfacial bonding and unstable interface are considered as the main factors limiting the applications of CNTs in AMNCs. In order to address these problems, it is necessary to regulate the interface: one possible solution is to introduce cladding suitable transient layer on CNTs surface, which can wet both CNTs and Al matrix, hinder interfacial reaction and reduce the gap of the mass density between CNTs and Al.

SiC has been studied as a promising candidate for the transition layer, showing good wettability with Al matrix [25, 28]. It was also found that SiC can stably exist in the process of preparing AMNCs by powder metallurgy [26], implying that a SiC transition layer can improve

wettability between CNTs and Al matrix as a transition layer. At the same time, SiC transition layer can prevent the direct contact between CNTs and Al matrix, hindering the adversely interfacial reaction; and it can also enhance the interfacial bonding by the formation of a covalent SiC bond [29]. In addition, the gap of mass density between CNTs and Al can be reduced by the heavier SiC decorating layer on the surface of CNTs, improving the dispersion homogeneity of CNTs in Al matrix [30]. However, the morphologies and structures of SiC layer are difficult to be effectively controlled: the SiC layer is prone to adhesion due to the transition reaction and it is still a challenge to obtain the composite phase with integrated structure and uniform dispersion [28-30]. These bottlenecks should be further studied then regulated to achieve high performance of CNTs reinforced AMNCs with good repeatability.

Few researches have documented improvement in interfacial wettability by SiC, enhancing the strengthening effect in CNTs reinforced AMNCs. T. Laha et al. investigated the wetting behavior and the interface between the hypereutectic Al-Si alloy and the MWCNTs in composite by thermal spray, and the formation of an ultrathin β -SiC reaction layer was found to be responsible for improving the wetting kinetics [29]. K.P. So coated SiC on the CNTs surface through a three-step process to improve the wettability of CNTs during Al melting [31]. The methodology presented in this study show significant overall improvement as compared to the previously reported results, benefitting from the good affinity and reactivity between silicon and CNTs. Based on the detailed interface study, we have demonstrated that through the proportion design and control of processing parameters, a continuous nano-SiC transition layer with controllable thickness was directly synthesized on the outer wall of CNTs by one-step heat treatment through solid state reaction to regulate the interfacial characteristic prior to mixing with Al powder in an innovative way. Thus, it can act as a good compatibility and wettability

intermediate phase between CNTs and Al matrix, forming a better bonding for load transfer as well as other physical and chemical information transmission [32-33]. The effects of SiC transition layer and its content on densification process, interfacial structure, mechanical and electrical properties of AMNCs will be discussed.

2. Experimental procedures

2.1 Synthesis of SiC-clad carbon nanotubes

Near-spherical nano Si powders (Purity >99.9 wt.%, diameter ~30 nm) were selected as the raw materials to synthesize nano SiC layer on the outer walls of MWCNTs (diameter ~150 nm, length 10~50 μm , density 2.0 g/cm^3). CNTs and Si powders were mixed by synchronized ultrasonic dispersion and mechanical stirring, while 1% polyvinyl pyrrolidone (PVP) was used as polymer surfactant to promote its uniform dispersion. The proportion of CNTs and Si powders was regulated to ensure the final volume ratio of CNTs to SiC equaling to 1:1 in as-obtained SiC-clad CNTs (simplified as CNTs/SiC) powders. Then, CNTs-Si powder mixtures were heated inside a vacuum furnace for 1 hour at different temperatures in the range of 1000~1300 $^{\circ}\text{C}$.

2.2 Application of CNTs/SiC composite reinforcements in AMNCs

The obtained CNTs/SiC composite powders were used as reinforcements to fabricate AMNCs. The schematic diagrams of preparation process of CNTs/SiC composite powders and its reinforced AMNCs are shown in Figure 1. Planetary ball milling (200 rpm for 4 hours) was performed to mix Al powders and as-prepared CNTs/SiC powders with different content (0.25, 0.5, 1.0 and 1.5% CNTs in volume fraction after reacted with Si) in argon gas condition. The powder mixtures were mixed with 2 wt.% ethanol which was used as process control agent, the ratio of ball to powders is 5:1 while the ZrO_2 milling balls ratio of 10 mm to 5 mm is 4:1. Then, spark plasma sintering (SPS) was used to consolidate the powder mixtures (sintering at 630 $^{\circ}\text{C}$

for 30 min with an applied pressure of 30 MPa in a vacuum of ~ 5 Pa). Finally, the as-sintered bulks were extruded into rods for tests at 400 °C with a reduction ratio of ~ 18 and a ram speed of 3 mm/s in a flowing Ar atmosphere. As a comparison, AMNCs reinforced by CNTs or nano SiC_p (Purity >99.9 wt.%, diameter ~ 30 nm) were also prepared following the same procedure. Near-spherical nano-SiC powders are shown in the supplementary materials (Figure S1). In addition, pure Al was chosen as a reference material.

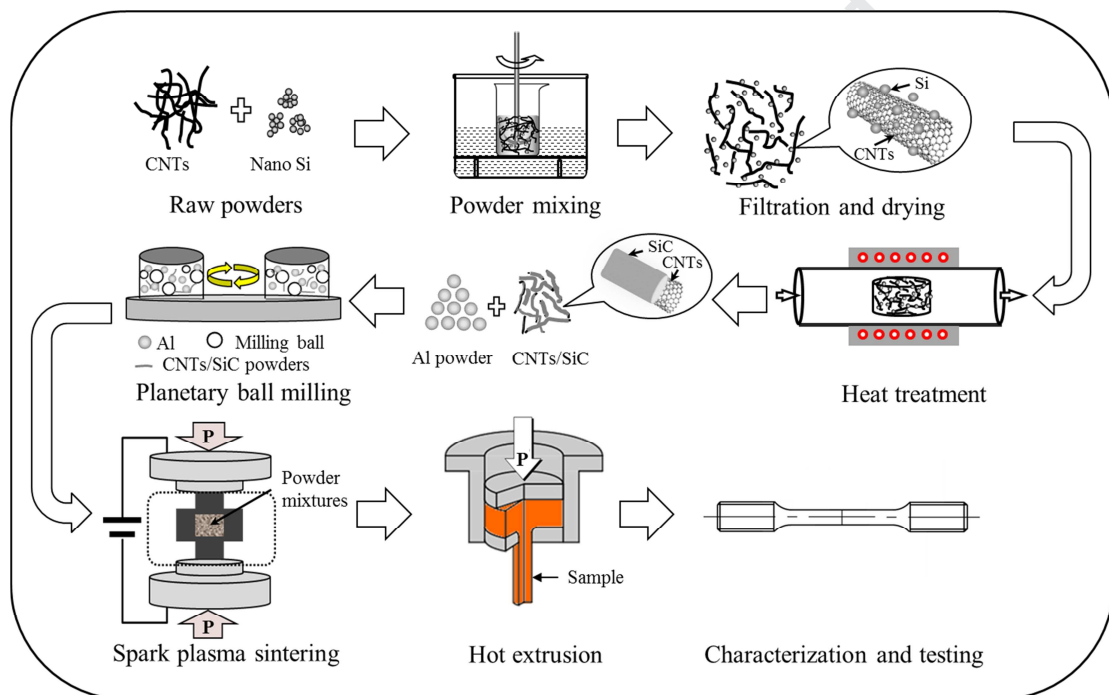


Figure 1. Schematic diagrams of preparation process of CNTs/SiC composite powders and it reinforced aluminum matrix nanocomposites (AMNCs).

2.3 Characterization of microstructure and evaluation of properties

The morphologies of CNTs-Si powder mixtures and as-prepared CNTs/SiC powders were characterized by a field emission scanning electronic microscope (FESEM, Merlin Compact, ZEISS, Germany), while an EDS detector (INCA X-Max, Oxford, UK) was attached to the FESEM to observe the distribution of the elements. A transmission electronic microscope (TEM,

JEM-2010, JEOL, Japan) was used to reveal the details of the microstructure and interface of CNTs/SiC powders and it reinforced AMNCs. Chemical bonding state of CNTs and CNTs/SiC were investigated by X-ray photoelectron spectroscopy (XPS) (AXISULTRA, Kratos, UK). X-ray diffraction (XRD-7000, SHIMADZU, Japan) was employed to confirm the phase compositions of the reinforcements and AMNCs with the scanning speed of 8°/min. The crystallographic structures of CNTs/SiC powders were tested by a microscopic laser Raman spectrometer (ARAMIS, HORIBA, Japan). Tensile tests were carried out in a universal testing machine (AGS-X, SHIMADZU, Japan), the strain rate chosen as $5 \times 10^{-4} \text{ s}^{-1}$. A portable eddy current tester (Sigma-2008B1, TIAN YAN, China) was used to detect the electrical conductivities of as-extruded materials.

3. Results and discussion

3.1 Morphologies of as-mixed CNTs-Si and CNTs/SiC composite powders

Morphologies and corresponding EDS mappings of as-mixed CNTs-Si powder before and after heat treatment at 1200 °C are analyzed to confirm the formation of SiC layer on the surface of CNTs. Figure 2a clearly shows that nano Si powders were uniformly dispersed on CNTs surface after synchronized ultrasonic dispersion and mechanical stirring before heat treatment. Nano Si powders reacted with outer walls of CNTs and formed a nearly continuous SiC transition layer on the surface of CNTs during the heat treatment, observing from the rough surface, as shown in Figure 2b. Figures 2c-e show the microstructures with the corresponding EDS mappings of CNTs/SiC covering the similar area after heat treatment. It can be seen that a nano layer existing on the surface of rod-like CNTs structures. The rich carbon content areas present the shape of fibrous structures, corresponding to the raw CNTs. Meanwhile, high concentration map of element Si shows a similar pattern, revealing CNTs clad by forming a

nano SiC layer.

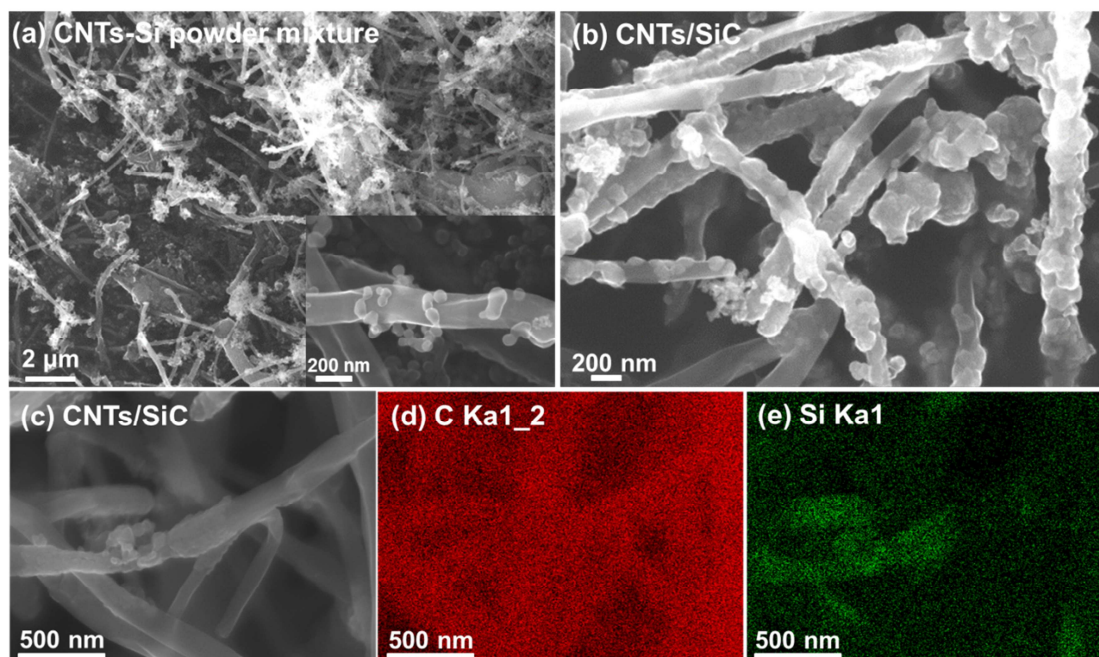


Figure 2. Scanning electrical microscope (SEM) images showing morphologies of powder mixtures. (a) CNTs-Si powder mixtures before heat treatment. (b, c) CNTs/SiC composite powders after heat treatment. (d, e) The corresponding EDS mapping showing the Carbon and Si distribution respectively covering the area in (c).

3.2 Interface, phase composition and formation mechanism of CNTs/SiC powders

TEM images with the corresponding selected area electron diffraction (SAED) pattern of CNTs/SiC powders after heat treatment at 1200 °C are shown in Figure 3. Meanwhile, more TEM micrographs of formed CNTs/SiC composite powders were indexed as supplementary material (Figure S2) to further support the results. It is obvious that SiC was synthesized on the surface of CNTs, while the majority of the internal parts of CNTs still maintained their original fibrous structure and component (Figures 3a-c and Figure S2). The interface between CNTs and SiC can be clearly observed through the high resolution TEM (HR-TEM, Figures 3d-e), where two different atom plane spaces (0.25 nm for area A2, A3 and A4, 0.34 nm for area A1 and A6 in

Figure 3d and 3e) on both sides of the interface are distinguished visibly, corresponding to the planes of (111) of SiC and (002) of CNTs, respectively [31, 34]. It confirms that area A5 in Figure 3e corresponding to CNTs-SiC junction region. The statistical thickness of SiC layer measured based on these experimental observations is 24.79 nm. Taking a simple assumption those CNTs rod-like structures covered by a nearly continuous SiC transition layer, the theoretical thickness of SiC layer with the volume ratio of CNTs to SiC as 1:1 is calculated to be 25 nm, which is in excellent agreement with the measured thickness. By adding SiC transition layer, the theoretical density of CNTs/SiC composite powder was found to be 2.6 g/cm^3 , a significant increase compared to the density of CNTs ($\sim 2.0 \text{ g/cm}^3$). The higher density of CNTs/SiC composite powder helps to reduce the specific gravity difference with Al matrix, promoting a uniform dispersion in Al matrix. Meanwhile, considering the cladding structure of CNTs/SiC composite reinforcement and the consumption of CNTs during the reaction procedure, multi-walled CNTs with large diameter were selected as raw materials at the beginning and CNTs were kept in excess state. The microstructures (Figure 2 and Figure 3) of CNTs/SiC display that the residual CNTs presents a diameter of about 100 nm, showing a small reduction as compared with the original CNTs. It was also indicated that the outer walls of CNTs were indeed consumed in the reaction process, but it still maintained a relatively complete structure and composition. Undoubtedly, the new combined structure (containing the SiC layer and residual CNTs) plays the key role in improving the mechanical performance of AMNCs, but it is hard to separate the individual strengthening contribution of CNTs and SiC layer.

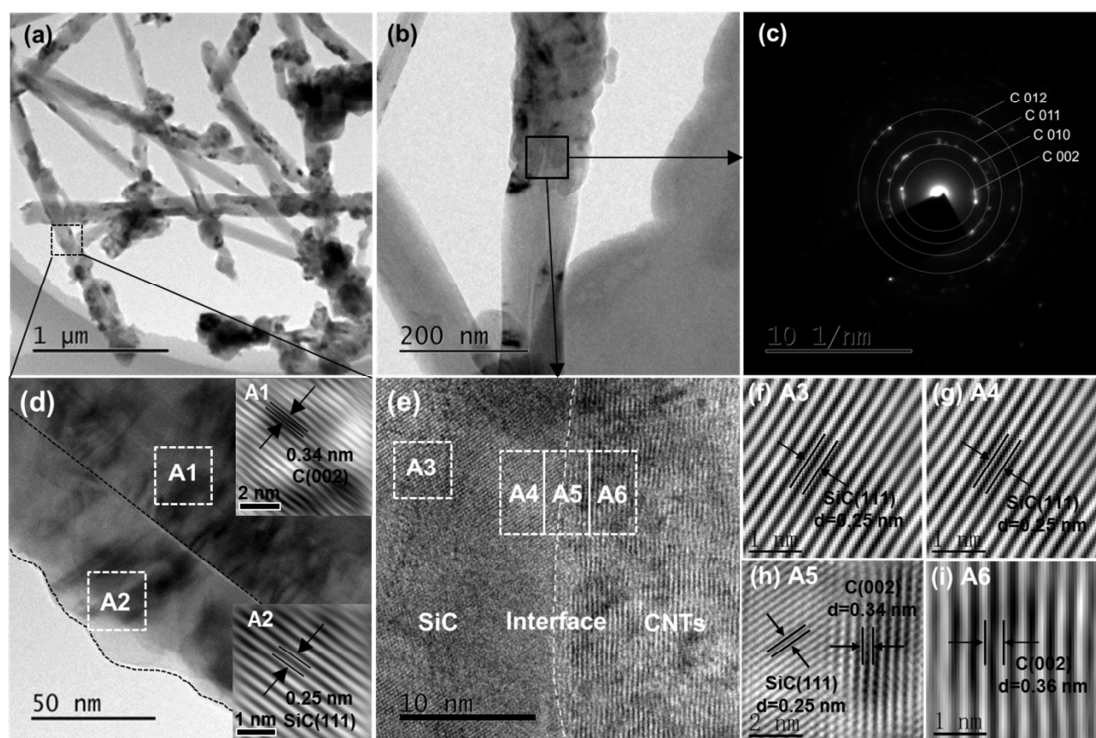


Figure 3. Microstructures and interfaces of CNTs/SiC powders. (a-c) TEM images and corresponding SAED of CNTs/SiC powders after heat treatment at 1200 °C. (d-i) HR-TEM images of CNTs/SiC and the atom planes corresponding to areas A1-A2 in (d), areas A3-A6 in (e).

The XRD patterns of CNTs-Si powder mixtures and CNTs/SiC powders after heat treatment at different temperatures in the range of 1000~1300 °C are shown in Figure 4. After heat treatment at 1000 °C, only the diffraction peaks of graphite and Si can be found in CNTs-Si powder mixtures. This suggests that there is no reaction yet between CNTs and Si at this temperature. The formation of SiC through interfacial reaction between CNTs and Si is detected when the temperature is above 1100 °C. The SiC diffraction peaks are detected at 35.7°, 60.1° and 72.0°, 41.5° and 75.7° corresponding to (111), (220), (311), (200) and (222) crystallographic planes of cubic β -SiC, respectively. Increasing the temperature further will assist this reaction, and nano Si powders are believed to be completely consumed by forming the SiC layer with the

outer walls of CNTs, evidenced by the strong SiC peaks appearing at 1200 °C and no residual diffraction peaks of Si. This also agrees with the morphological results in Figure 2 and Figure 3, and the formation of SiC layer seems not compromise the structure and composition of the core of CNTs.

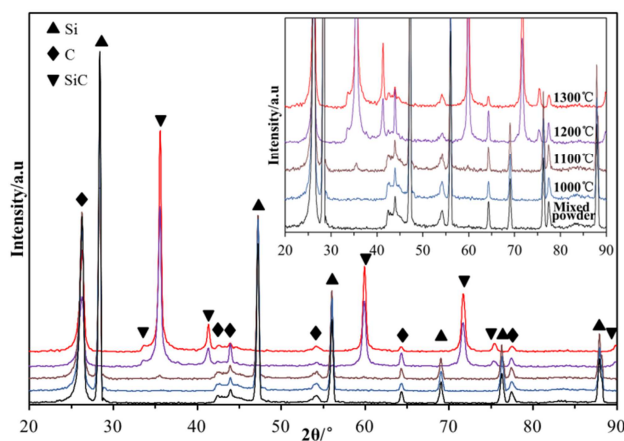


Figure 4. X-ray diffraction (XRD) patterns of CNTs-Si powder mixtures and CNTs/SiC composite powders after heat treatment at four different temperatures 1000, 1100, 1200 and 1300 °C.

The XPS results of original CNTs and CNTs/SiC after 1200 °C heat treatment are shown in supplementary material (Figure S3) and Figure 5. The charge neutralizer was used to compensate for surface charge effects, and binding energies were calibrated using the C 1s hydrocarbon peak at 284.8 eV. Figure S1a shows that two primary XPS peaks are observed clearly in original CNTs, corresponding to the peaks of C 1s and O 1s, respectively. Five C 1s peaks are displayed in Figure S1b, with fitted peak values at about 280.8, 282.6, 284.3, 286.0 and 287.8 eV, corresponding to the sp^2 and sp^3 of C-C, C-O, C=O and O-C=O band respectively [35, 36]. Figure S1c shows a sub-peak of O 1s at about 528.6 eV, corresponding to the chemisorbed oxygen. Figure 5a reveals the XPS spectra of CNTs/SiC, C, Si and O band can be detected clearly after heat treatment. Besides the photoelectron peaks of C 1s (281.3, 283.1 and 285.0 eV

for sp^2 , sp^3 and C-O band, respectively, Figure 5c) and O 1s (529.1 eV, Figure 5d), Si 2s and Si 2p XPS peaks can also be identified. Two strong bands of Si 2p (Figure 5b) at about 97.9 and 99.7 eV can be ascribed to the Si-C and Si-O band, which strongly indicates the formation of SiC [33, 35]. In addition, both C 1s and O 1s peaks have a 0.5 eV integral shift to high binding energy compare with raw CNTs, normally caused by the formation of new bonds and changes in the environment around atoms. It is believed that C=O and O-C=O band were completely destroyed, which implies that the reaction between CNTs and Si preferentially occurred at CNTs defects, because those area containing more active groups after acidizing treatment [33]. It can be concluded from the observation evidence that the composite structure of CNTs/SiC were synthesized on the surface of CNTs by the proposed method.

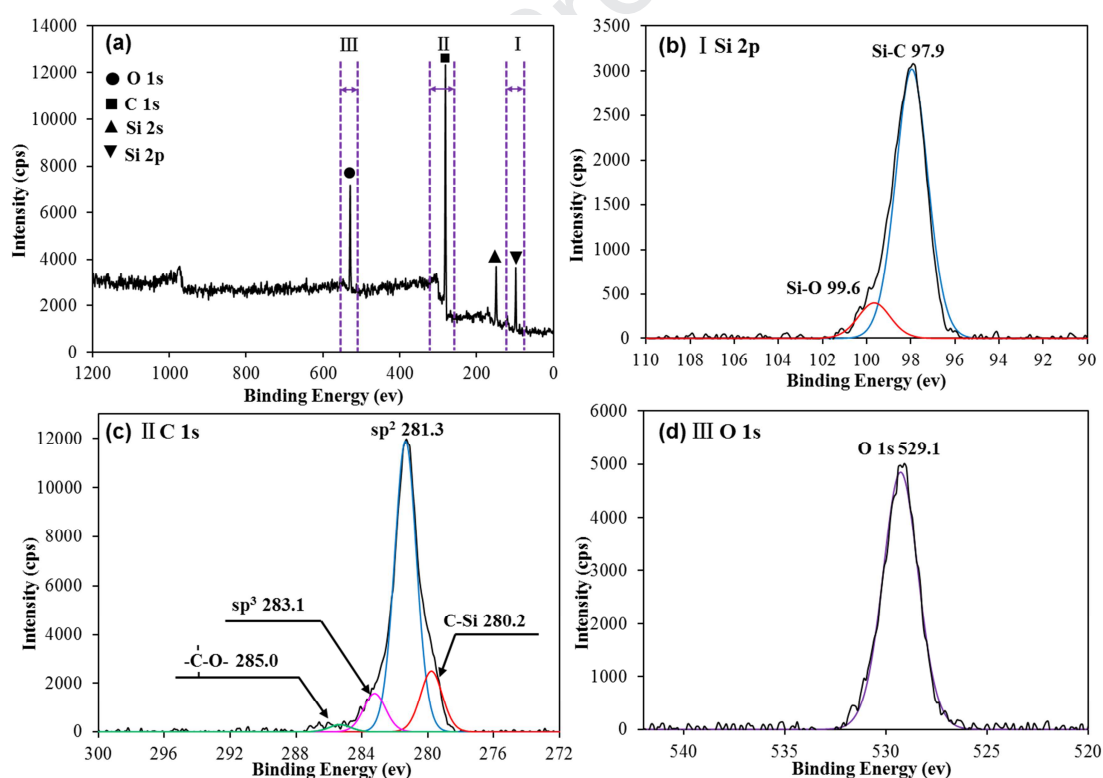
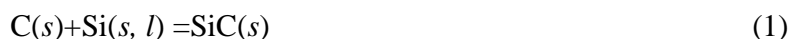


Figure 5. (a) XPS results of CNTs/SiC reinforcement after 1200 °C heat treatment. (b, c, d) XPS pattern of Si 2p, C 1s and O 1s band respectively.

Figure 6 shows the variation of Gibbs free energy with temperature and schematic diagram of formation mechanism of SiC layer on CNTs surface synthesized from CNTs-silicon reaction. The reaction between CNTs and silicon is described below:



Calculations according to Equation (1) confirm that the Gibbs free energy (ΔG) of formation for SiC phase by solid-solid reaction (<1685 K) and solid-liquid reaction (>1685 K) between graphite and silicon are negative. This indicates that the SiC formation from CNTs-silicon reaction is thermodynamically favorit. It is believe that the formation of SiC begins at the active site on CNTs defects, and the solid state reaction mainly depends on the diffusion of carbon atoms through the interstitial sites and Si atoms by vacancy migration in regular silicon sites [29]. Thus, silicon and carbon atoms diffusion each other through the formed SiC layer, reaches the interface of carbon-silicon carbide and reacts to form a continuous β -SiC reaction layer [37]. However, the formation of SiC layer limits the further atom diffusion, as a result, SiC prefers to grow in the axial direction (parallel to CNTs axis) than the radial direction (vertical to CNTs axis) [29, 38]. Furthermore, the close-packed plane of β -SiC is {111} and its surface energy is the lowest, which is conducive to the directional preferential growth of SiC. This is confirmed by the HR-TEM micrographs (Figure 3d, Figure S2 and Figure 6): SiC can achieve <111> directional growth in the axial direction by stacking atoms on this plane to maintain minimum energy requirements.

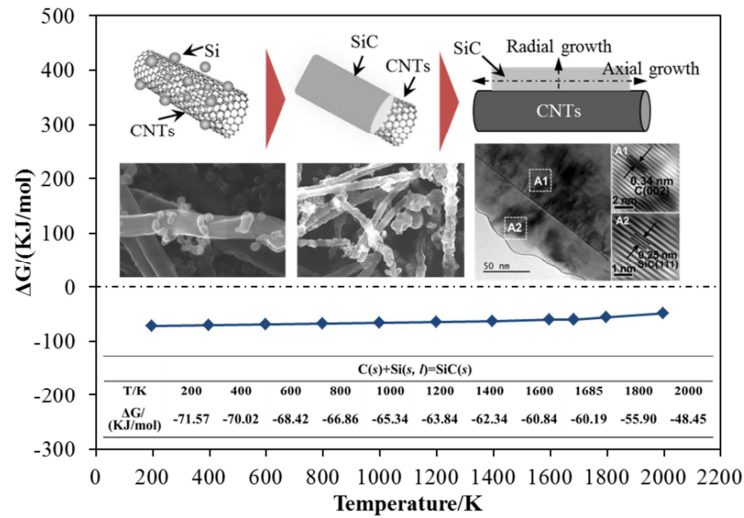


Figure 6. Thermodynamic analysis results and schematic diagram of formation mechanism of SiC layer synthesized from carbon-silicon reaction.

3.3 Analysis of phase composition of AMNCs

After consolidating the CNTs/SiC-Al powder mixtures, the phase compositions were studied to analyze the interfacial reaction in AMNCs. XRD patterns of pure Al, CNTs reinforced AMNCs (CNTs-Al) and CNTs/SiC reinforced AMNCs (CNTs/SiC-Al) are shown in Figure 7. Graphite peak can be detected at 26.6° in CNTs-Al and CNTs/SiC-Al, and distinct Al_4C_3 peaks can only be found at about 31.7° , 40.2° and 55.1° in CNTs reinforced AMNCs. Slight SiC diffraction peaks are detected at 35.7° , 60.1° and 72.0° , corresponding to (111), (220) and (311) crystallographic planes of β -SiC, respectively [39, 40]. This result implies that SiC remains as a transition layer on CNTs surface in AMNCs preventing the formation of Al_4C_3 phase.

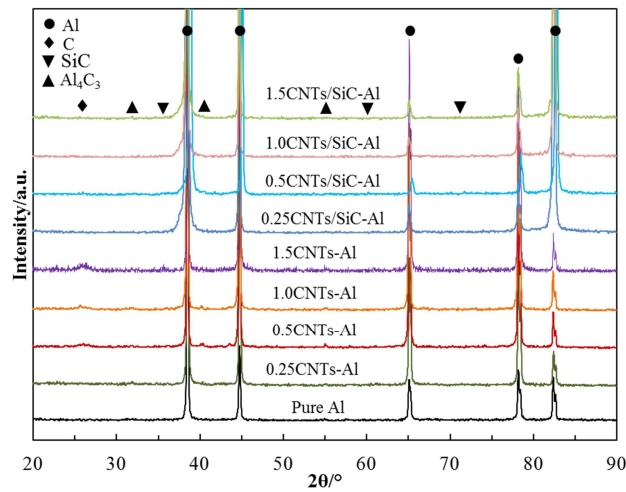


Figure 7. XRD patterns of pure Al, CNTs and CNTs/SiC reinforced AMNCs.

The Raman spectra obtained from the area of primary particle boundaries and CNTs clusters in AMNCs are shown in Figure 8. Strong Al_4C_3 peaks can be found at 485 cm^{-1} and 855 cm^{-1} in CNTs reinforced AMNCs [41], confirming the interfacial reaction between CNTs and Al matrix during consolidation. The Raman results obtained from CNTs/SiC reinforced AMNCs also show no-existence of Al_4C_3 reaction phase, and SiC peaks were found at 796 cm^{-1} and 972 cm^{-1} . Furthermore, Raman peaks of CNTs still survive at 1344 cm^{-1} and 1576 cm^{-1} in CNTs/SiC reinforced AMNCs, indicating that Si reacted with the outer walls of CNTs, and the core still maintained its original structure and composition (also see Figure 2). These results indicate that, as a transition layer, SiC formed on the surface of CNTs effectively regulates the interfacial reaction, which hinders the generation of easily hydrolyzed brittle phase Al_4C_3 . Moreover, the SiC transition layer provides a stronger interfacial bonding between CNTs and Al matrix by the formation of a covalent Si-C bond, advantaging to the CNTs strengthening effect by achieving high load transfer efficiency [42, 43].

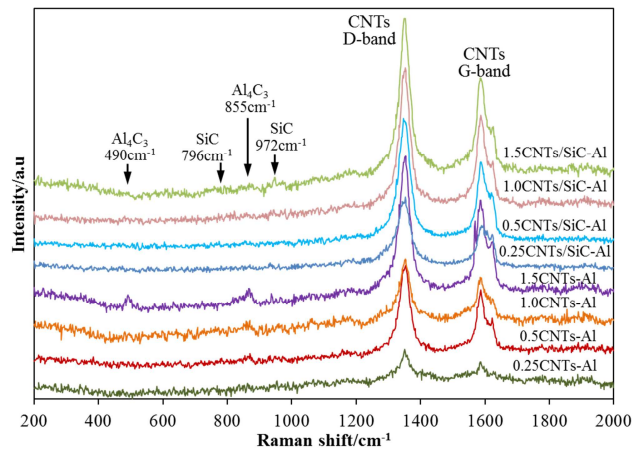


Figure 8. Raman spectra of CNTs or CNTs/SiC reinforced AMNCs.

3.4 Microstructure and interface of AMNCs

The interfacial structure of CNTs/SiC/Al was observed to evaluate the effect of SiC on the interfacial reaction and bonding between CNTs and Al matrix. Figures 9a-c show TEM images with corresponding SAED of 1.0CNTs-Al. It can be seen that there is an obvious interface reaction layer between CNTs and Al matrix. The corresponding SAED patterns (Diff. 1 and Diff. 2) also suggest that Al_4C_3 layer is formed through the interfacial reaction. Combining the results of XRD pattern and Raman spectra, it can be preliminarily concluded that the interface product (Al_4C_3) is formed in CNTs reinforced AMNCs, but the inner walls of CNTs still maintain its original structure and component. CNTs/SiC reinforcements are dispersed individually in AMNCs as observed from the bright field (BF, Figure 9d) and dark field image (DF, Figure 9e). Magnifying image (Figure 9f) shows that CNTs/SiC displays the hollow rod-like microstructure in AMNCs which resembles to its composite powder, and SiC acts as a transition layer on the surface of CNTs. HR-TEM images (Figures 9g-h) show the biphasic interfaces between CNTs-SiC and SiC-Al. The atom planes (002) (0.36 nm) of CNTs, (111) (0.25 nm) of SiC and (111) (0.23 nm) of Al of the different districts in Figure 9h are observed. The phases of different areas in Figure 9h are identified by SAED (Diff. 3 and Diff. 4). Diffraction spots of CNTs and SiC are

confirmed, and no interfacial reaction phase is found. These results provide further evidence that CNTs/SiC reinforcements fundamentally inhibit the Al_4C_3 formation in AMNCs.

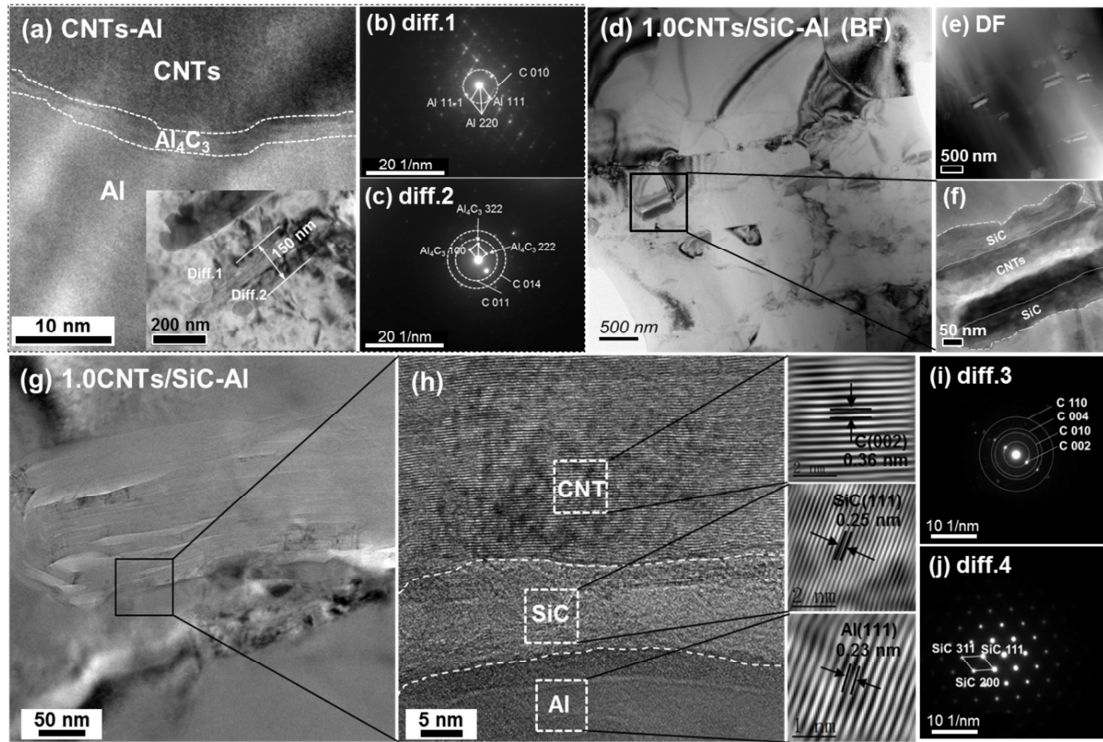


Figure 9. TEM images with the corresponding SAED of CNTs-Al and 1.0CNTs/SiC-Al. (a) A bright TEM image of 1.0CNTs-Al. (b, c) SAED patterns of area Diff.1 and Diff.2 in (a). (d-g) Bright and dark TEM image of 1.0CNTs/SiC-Al. (h) HR-TEM image in (g). (i-j) Corresponding SAED to image (h).

3.5 Strengthening effect of CNTs/SiC in AMNCs

Table 1

Summary of mechanical and electrical performance of pure Al and various AMNCs (enhanced by CNTs, SiC and CNTs/SiC)

Materials	Relative density/%	YS/MPa	UTS/MPa	Elongation /%	Conductivity /IACS%
Pure Al	99.88	106.2	127.1(\pm 2.1)	29.8	58.0
0.25CNTs-Al	99.41	133.4	163.5(\pm 1.5)	19.5	54.4
0.5CNTs-Al	99.57	121.3	152.7(\pm 3.3)	18.3	52.3

1.0CNTs-Al	99.43	108.3	148.3(\pm 1.0)	16.2	51.9
1.5CNTs-Al	99.28	103.9	138.3(\pm 1.2)	15.2	45.9
0.25SiC-Al	99.86	131.8	158.6(\pm 1.7)	28.0	57.2
0.5SiC-Al	99.79	131.2	157.7(\pm 1.6)	28.5	54.1
1.0SiC-Al	99.63	132.0	157.0(\pm 2.5)	29.7	53.9
1.5SiC-Al	99.72	129.5	155.0(\pm 2.1)	25.6	52.0
0.25CNTs/SiC-Al	99.85	125.7	176.6(\pm 1.5)	25.3	54.6
0.5CNTs/SiC-Al	99.46	122.3	181.2(\pm 3.2)	19.5	53.6
1.0CNTs/SiC-Al	99.78	161.1	198.8(\pm 2.4)	19.0	52.4
1.5CNTs/SiC-Al	99.42	120.1	173.5(\pm 3.7)	17.6	50.6

The mechanical tests of pure Al and AMNCs were carried out to evaluate the strengthening effect of the reinforcement. The corresponding test results are summarized in table 1. The stress-strain curves of AMNCs containing 1.0 vol.% reinforcements (CNTs, SiC or CNTs/SiC) are shown in Figure 10a. The yield strength (YS) and ultimate tensile strength (UTS) of 1.0CNTs reinforced AMNCs were measured as 110 MPa and 148 MPa, respectively. However, its elongation decreases to 16.2%. The strength of 1.0SiC reinforced AMNCs reaches 157 MPa in UTS in combination with a good elongation (29.7%). This can be attributed to the reasons, i.e. Nano SiC hardly splits and reduces the continuity and flexibility of the matrix structure [44]; SiC particle is easy to cooperate with matrix plastic deformation duo to the small size, which can greatly reduce the probability of premature failure of composites at large size reinforced particles [45, 46]; in the process of tension, the stress concentration produced by near spherical particles is less than that of the particles with larger aspect ratio, it may effectively reduce the initiation and propagation of cracks caused by stress concentration. Therefore, nano SiC particle is very unfavorable to the elongation [47], preserving the good ductility of Al matrix. It is clear that 1.0CNTs/SiC reinforced AMNCs shows further improved synthetically mechanical properties: YS and UTS reach 161 MPa and 199 MPa respectively, 41.5% and 55.9% stronger than pure Al respectively (106 MPa for YS and 127 MPa for UTS). The improvement in strength is mainly attributed to the effectively load transfer to CNTs by the strong interfacial bonding between

CNTs/SiC and Al matrix [48]. In addition, the existence of SiC layer effectively inhibits the interfacial reaction, and further improves the mechanical properties and structural stabilities of AMNCs without reducing their ductility significantly compared with CNTs reinforced AMNCs, [26, 49], as shown in Figure 10b and 10c. Table 1 and Figure 10b also show that the strengths of CNTs/SiC reinforced AMNCs increase constantly when the increase of CNTs content (except the sample of 1.5 vol.%), while the performance of CNTs reinforced AMNCs and SiC reinforced AMNCs decline or stay the same level with the increase of the reinforcements content.

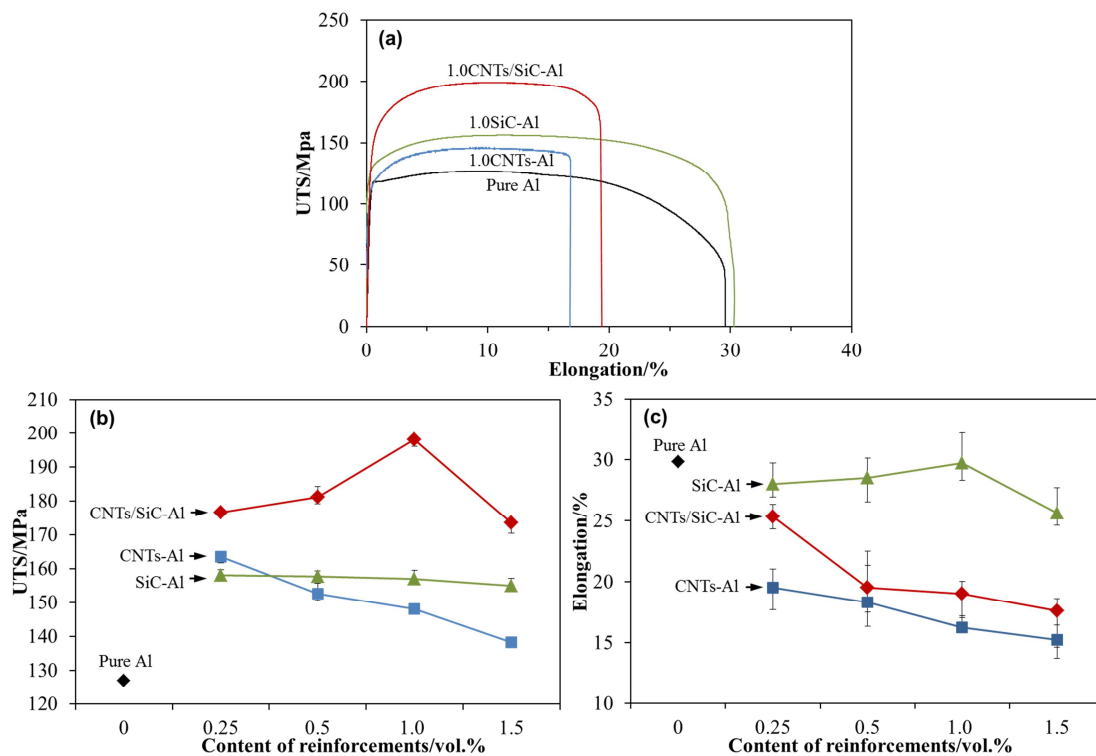


Figure 10. The stress-strain curves and mechanical properties of AMNCs. (a) Stress-strain curves of pure Al and AMNCs with 1.0vol% reinforcement (CNTs, nano SiC or CNTs/SiC). (b) Strength of various AMNCs. (c-d) Elongation curves of various AMNCs.

At the end of tensile test, the fracture surfaces of CNTs reinforced AMNCs are shown in Figure 11a and b. A large number of dimples appear in the fracture, proving the ductile fracture

in Al matrix. However, in addition to the fractured CNTs distribute in Al matrix dimples, a small amount of CNTs clusters (denoted as CNT ①) are pulled out directly from the Al matrix, i.e., they are debonded with the matrix because of the weak interfacial bonding. It implies that the agglomeration of CNTs fails to transfer load from matrix to CNTs, and also could lead to defects during loading, causing premature failure of materials. Figure 11c shows the corresponding failure diagram of CNTs in Al matrix. The ruptured and non-debonding CNTs/SiC tensile fractures are observed on the fracture surface of AMNCs reinforced with CNTs/SiC (Figure 11d and 11e), matching the expected uniform dispersion. This also corroborates our initial expectation that the SiC cladding layer is conducive to reducing the mass density difference and specific surface energy, improving the dispersion of CNTs in matrix. The peeled CNTs/SiC (denoted as CNTs/SiC ② and ③) and a tearing CNTs/SiC (denoted as CNTs/SiC ④) are also observed, as shown in Figure 11e. CNTs/SiC ② and ③ show one-time peeling morphology with a clear transition slope. And it is accompanied by a significant change in diameter as an arrow indicated in Figure 11e. The morphology schemes of the peeling of CNTs/SiC are shown in Figure 11f. The breaking and interlaminar peeling of CNTs/SiC indicates a good interface bonding between reinforcements and Al matrix. A large number of well-distributed dimples also support the ductile fracture. It suggests that the interface between CNTs/SiC and Al matrix is firmly bonded, improving load transfer from the matrix to reinforcements. As reported, the contact angle is used to estimate the wettability and bonding between the reinforcement and matrix which defined by a sessile drop method [50]. More details are included in supplementary material. In So's study [31], Al droplets were dropped on the surface of CNTs and CNTs/SiC pellet to test the contact angle. The average contact angle of Al droplet and CNTs (145.8°) is larger than that of Al droplet and CNTs/SiC (134.6°) [25, 51]. The

interfacial bonding force was reflected by the work of adhesion (Π_a) of Al liquid and reinforcement according to Young-Dupre equation [52]

$$\Pi_a = \gamma_{lv}(1 + \cos\theta) \quad (2)$$

Where γ_{lv} is the specific energy of liquid-vapor interface ($\approx 850 \text{ mJ/m}^2$) [53]. The values of Π_a are estimated to 200 mJ/m^2 for CNTs and 1300 mJ/m^2 for CNTs/SiC at 1100 K [25], respectively. It indicates that the improvements of wettability and interface bonding between CNTs and Al matrix are attributed to the covalent bonding from the introduction of nano SiC transition layer on CNTs surface, which is favorable for improving the efficiency of load transfer from Al matrix to CNTs. For instance, the strong interfacial bonding also provides a good ductility as shown in Figure 10c by transferring the load from matrix to reinforcements.

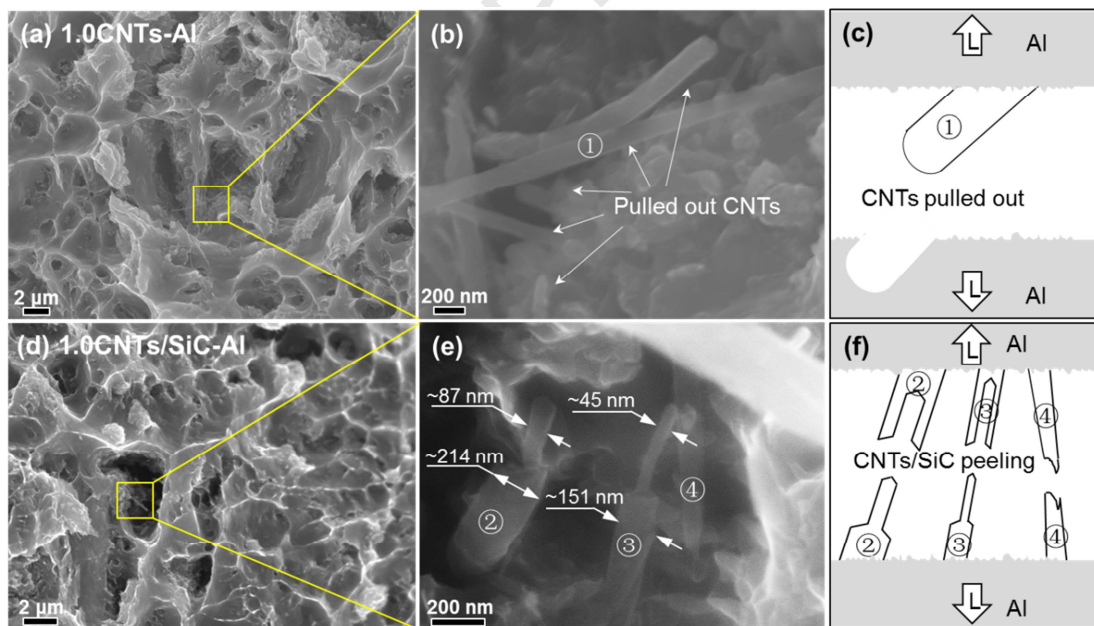


Figure 11. The fracture surfaces and the failure diagrams of CNTs, CNTs/SiC reinforced AMNCs. (a, b) The fracture surfaces of CNTs reinforced AMNCs with 1.0vol% reinforcement. (c) CNTs failure diagram corresponding to (a) and (b). (d, e) The fracture surfaces of 1.0CNTs/SiC reinforced AMNCs. (f) CNTs/SiC failure diagram corresponding to (d) and (e).

A summary of the measured of electrical conductivity data from different AMNCs enhanced by various reinforcements (CNTs, SiC or CNTs/SiC) at different volume fractions (0.25, 0.5, 1.0 and 1.5 vol.%) is shown in Figure 12 and Table 1. It can be seen that the overall trend of conductivity of AMNCs decreases gradually with the increase of the content of reinforcement due to the more scattering of electrons by the interface [54], especially for the CNTs reinforced AMNCs. This mainly related to the poor interface bonding, the aggregation of CNTs and the formation of Al_4C_3 in Al matrix. Nano SiC reinforced AMNs show relatively better conductivity, even close to pure Al (58.0 %IACS), due to the good wettability and interface bonding between SiC and Al matrix. In addition, nano-scale SiC particles will not split and reduce the continuity of the matrix structure, thus the good conductivity of metal Al can be well preserved. After cladding the nano SiC layer on the surface of CNTs, the wettability and interface bonding is improved and the dispersion of CNTs is promoted by reducing the specific mass difference and specific surface energy at the same time [26, 54]. Therefore, AMNCs reinforced with CNTs/SiC show an intermediate conductivity in comparison with CNTs or SiC reinforced AMNCs in the same content of reinforcements. Nevertheless the conductivity values of CNTs/SiC reinforced AMNCs can be maintained above 50%IACS.

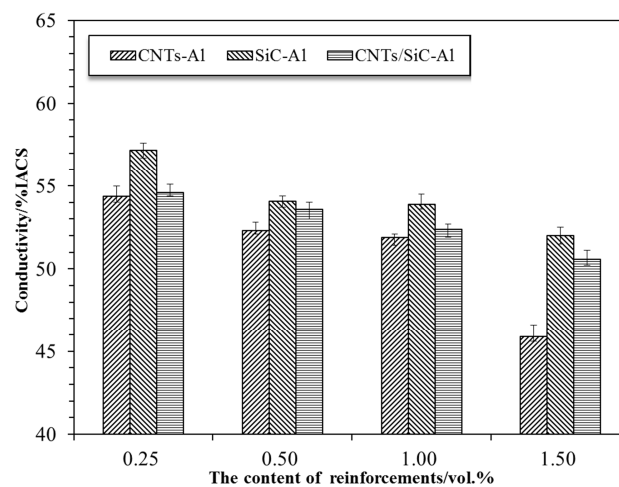


Figure 12. The electrical conductivity of AMNCs reinforced with various reinforcement (CNTs, nano SiC or CNTs/SiC) at different volume fractions (0.25, 0.5, 1.0 and 1.5 vol.%).

In summary, nano SiC transition layer was synthesized from the reaction between CNTs and nano Si. It was proved that the thickness and structure of CNTs/SiC composite reinforcement can be designed and controllably prepared. As a compatibility nano transition layer, SiC-clad CNTs improve the wettability and interfacial bonding between the reinforcement and matrix, which is favorable to reduce the agglomeration trend of CNTs caused by Van der Waals force and regulate the adverse interfacial reaction. As the reinforcement content increases, the performance of CNTs/SiC reinforced AMNCs increases first and then decreases when the CNTs/SiC content exceed 1.0 vol.%, while the mechanical properties of AMNCs enhanced with CNTs decline constantly. The ductility and electrical conductivity of CNTs/SiC-Al are also improved in comparison with CNTs-Al in the same reinforcement content. Meanwhile, the strengthening mechanism of CNTs reinforced metal matrix composites has been investigated in previous studies and the results show that the strengthening effect of AMNCs is mainly contributed to impactful load transfer from matrix to CNTs, which is closely related to the firm interfacial bonding between CNTs and matrix [55-58]. The major compound of CNTs survived after reacting with Si powder which observed from the micrographs (Figure S2 and Figure 3). CNTs still presents the primitive fibrous structures. Moreover, the characteristic of the fracture surfaces of CNTs/SiC reinforced AMNCs shows interlaminar peeling morphology with a clear transition slope (see Figures 11e-f), further supporting the argument that the improvement in strength is mainly attributed to the effectively load transfer to CNTs by the strong interfacial bonding between CNTs/SiC and Al matrix. In additional, the movement of the dislocation when plastic deformation occurs in Al matrix can be hindered by nano CNTs/SiC composite reinforcements.

Generally, the mechanical properties of CNTs/SiC reinforced AMNCs are further improved without reducing its ductility. There is a slight reduction of electrical conductivity, but still a significant improvement when compared to CNTs only reinforced AMNCs.

4. Conclusions

The proposed methods in this study and fundamental understanding show the ability to design and improve the characterization of CNTs/SiC reinforced AMNCs by controlling the SiC transition layer. SiC was synthesized from carbon-silicon reaction as a compatibility transition layer on the surface of CNTs prior to mixing with Al powders. The actual thickness (24.79 nm) of formed SiC cladding layer is very close to its theoretical calculation (25 nm). It is found that the existence of SiC layer effectively regulates the interfacial reaction between CNTs and Al matrix, which hinders the generation of easily hydrolyzed Al_4C_3 phase. In addition, the SiC transition layer reduces the specific surface energy and the gap of mass density between CNTs and matrix. The results reported in this study suggest the interfacial bonding between CNTs and Al matrix make strong contribution to the strengthening effect of CNTs by achieving high load transfer efficiency. Comparing with CNTs or nano SiC reinforced AMNCs, CNTs/SiC reinforced AMNCs show remarkably better mechanical properties. In addition, the ductility and conductivity of CNTs/SiC enhanced AMNCs are also maintained at a reasonable high level.

Acknowledgments

This work was supported by the financial of the National Natural Science Foundation of China (Grant numbers 51571160 and 51871180); Xi'an Science and Technology Project (Grant number 201805037YD15CG21(15)); Natural Science Basic Research Plan in Shaanxi Province of China (Grant number 2015JM5233) and Xi'an University of Technology Doctoral Dissertation Innovation Fund (Grant number 310-252071903).

Appendix A. Supplementary material

The supplementary material file includes: SEM image of near-spherical nano-SiC powders (Figure S1); TEM micrographs of formed CNTs/SiC composite powders (Figure S2); XPS result of raw CNTs (Figure S3); more details about the estimation of the wettability and interfacial bonding between the reinforcement and matrix.

References

- [1] S. Yadav, S. Gangwar, S. Singh. Micro/Nano Reinforced Filled Metal Alloy Composites: A Review Over Current Development in Aerospace and Automobile Applications. *Materials Today: Proceedings* 4 (2017) 5571-5582.
- [2] Anthony Xavier M, Ajith Kumar J P. Machinability of Hybrid Metal Matrix Composite - A Review. *Procedia Engineering* 174 (2017) 1110-1118.
- [3] A. Azarniya, A. Azarniya, S. Sovizi, H. Reza M. Hosseini, T. Varol, A. Kawasaki, S. Ramakrishna. Physicomechanical properties of spark plasma sintered carbon nanotube-reinforced metal matrix nanocomposites. *Prog. Mater. Sci.* 90 (2017) 276-324.
- [4] Yashpal, Sumankant, C.S.Jawalkar, A.S. Verma, N.M. Suri. Fabrication of Aluminium Metal Matrix Composites with Particulate Reinforcement: A Review. *Materials Today: Proceedings* 4 (2017) 2927-2936.
- [5] B. Peng, M. Locascio, P. Zapol, S. Li, S.L. Mielke, G.C. Schatz, H.D. Espinosa. Measurements of near-ultimate strength for multiwalled carbon nanotubes and irradiation-induced crosslinking improvements. *Nat. Nanotechnol.* 3 (2008) 626-631.
- [6] M.F. Yu, O. Lurie, M.J. Dyer, K. Moloni, T.F. Kelly, R.S. Ruoff. Strength and breaking mechanism of multiwalled carbon nanotubes under tensile load. *Science* 287 (2000) 637-640.

- [7] M.F. De Volder, S.H. Tawfick, R.H. Baughman, A.J. Hart. Carbon nanotubes: present and future commercial applications. *Science* 339 (2013) 535-539.
- [8] L.F. Mondolfo. *Aluminum alloys: structure and properties*, Elsevier 2013.
- [9] L. Jiang, Z.Q. Li, G.L. Fan, L.L. Cao, D. Zhang. The use of flake powder metallurgy to produce carbon nanotube (CNT)/aluminum composites with a homogenous CNT distribution. *Carbon* 50 (2012) 1993-1998.
- [10] S.R. Bakshi, Agarwal A. An analysis of the factors affecting strengthening in carbon nanotube reinforced aluminum composites. *Carbon* 49 (2011) 533-544.
- [11] C.F. Deng, X.X. Zhang, Y.X. Ma, D.Z. Wang. Fabrication of aluminum matrix composite reinforced with carbon nanotubes. *Rare Metals* 26(5) (2007) 450-455.
- [12] J.H. Nie, C.C. Jia, N. Shi, Y.F. Zhang, Y. Li, X. Jia. Aluminum matrix composites reinforced by molybdenum-coated carbon nanotubes. *International journal of materials, metallurgy and materials* 18(6) (2011) 695-702.
- [13] Z.J. Zhang, Z. Sun, Y.W. Chen. Improve the field emission uniformity of carbon nanotubes treated by ball-milling process. *Appl. Surf. Sci.* 253(6) (2007) 3292-3297.
- [14] X.D. Yang, C.S. Shi, C.N. He, E.Z. Liu, J.J. Li, N.Q. Zhao. Synthesis of uniformly dispersed carbon nanotube reinforcement in Al powder for preparing reinforced Al composites. *Composites: Part A* 42 (2011) 1833-1839.
- [15] F.T. Fisher. *Nanomechanics and the Viscoelastic Behavior of Carbon Nanotubes Reinforced Polymers*, PhD Thesis. Northwestern University USA (2002) 85-87.
- [16] X.Q. Liu, C.J. Li, J. Eckert, K.G. Prashanth, O. Renk. Microstructure evolution and mechanical properties of carbon nanotubes reinforced Al matrix composites. *Mater. Charact.* 133 (2017) 122-132.

- [17] B. Chen, S. Li, H. Imai, L. Jia, J. Umeda, M. Takahashi, K. Kondoh. An approach for homogeneous carbon nanotube dispersion in Al matrix composites. *Mater. Design.* 72 (2015) 1-8.
- [18] S.C. Tjong. Recent progress in the development and properties of novel metal matrix nanocomposites reinforced with carbon nanotubes and graphene nanosheets. *Mater. Sci. Eng. R* 74 (2013) 281-350.
- [19] M.L. Chen, G.L. Fan, Z.Q. Tan, D.B. Xiong, Q. Guo, Y.S. Su, J. Zhang, Z.Q. Li, M. Naito, D. Zhang. Design of an efficient flake powder metallurgy route to fabricate CNT/6061Al composites. *Mater. Design* 142 (2018) 288-296.
- [20] C. He, N. Zhao, C. Shi, X. Du, J. Li, H. Li, Q. Cui. An approach to obtaining homogeneously dispersed carbon nanotubes in Al powders for preparing reinforced Al-matrix composites. *Adv. Mater.* 19 (2007) 1128-1132.
- [21] B. Chen, J. Shen, X. Ye, H. Imai, M. Takahashi, K. Kondoh. Solid-state interfacial reaction and load transfer efficiency in carbon nanotubes (CNTs)-reinforced aluminum matrix composites. *Carbon* 114 (2017) 198-208.
- [22] C.F. Deng, X.X. Zhang, D.Z. Wang, Q. Lin, A.B. Li. Preparation and characterization of carbon nanotubes/aluminum matrix composites. *Mater. Lett.* 61(8-9) (2007) 1725.
- [23] H.J. Choi, G.B. Kwon, G.Y. Lee, D.H. Bae. Reinforcement with carbon nanotubes in aluminum matrix composites. *Scr. Mater.* 59(3) (2008) 360.
- [24] H. Kurita, M. Estili, H. Kwon, T. Miyazaki, W. Zhou, J.F. Silvain, A. Kawasaki. Load bearing contribution of multi-walled carbon nanotubes on tensile response of aluminum. *Composites: Part A* 68 (2015) 133-139.
- [25] K. Landry, S. Kalotgeropoulou, N. Eustathopoulos. Wettability of carbon by aluminum and

- aluminum alloys. *Mater. Sci. Eng. A.* 254 (1998) 99.
- [26] X. Zhang, S.F. Li, D. Pan, B. Pan, K. Kondoh. Microstructure and synergistic-strengthening efficiency of CNTs-SiC_p dual-nano reinforcements in aluminum matrix composites. *Composites: Part A* 105 (2018) 87-96.
- [27] L. Ci, Z. Ryu, N.Y. Jin-Phillip, M. Rühle. Investigation of the interfacial reaction between multi-walled carbon nanotubes and aluminum. *Acta Mater.* 54 (2006) 5367-5375.
- [28] V. Laurent, C. Rado, N. Eustathopoulos. Wetting kinetics and bonding of Al and Al alloys on a-SiC. *Mater. Sci. Eng. A: Struct.* 205 (1996) 1.
- [29] T. Laha, S. Kuchibhatla, S. Seal, W. Li, A. Agarwal. Interfacial phenomena in thermally sprayed multiwalled carbon nanotube reinforced aluminum nanocomposite. *Acta Mater.* 55 (2007) 1059-1066.
- [30] I.H. Kim, W. Lee, C.W. Lee, S.H. Ko, J.M. Jang. Effect of SiC coating on interfacial reaction between carbon short fiber and Al melt. *Surf. Interface Anal.* 42 (2010) 743.
- [31] K.P. So, J.C. Jeong, J.G. Park, H.K. Park, Y.H. Choi, D.H. Noh, Dong Hoon Keum, H.Y. Jeong, C. Biswas, C.H Hong, Y.H. Lee. SiC formation on carbon nanotube surface for improving wettability with aluminum. *Compo. Sci. Technol.* 74 (2013) 6-13.
- [32] H. Kwon, M. Leparoux, A. Kawasaki. Functionally graded dual-nanoparticulate-reinforced aluminum matrix bulk materials fabricated by spark plasma sintering. *J. Mech. Sci. Technol.* 30(8) (2014) 736-742.
- [33] L.P. Rajukumar, M. Belmonte, J.E. Slimak, A.L. Elías, E.C. Silva. 3D Nanocomposites of Covalently Interconnected Multiwalled Carbon Nanotubes with SiC with Enhanced Thermal and Electrical Properties. *Adv. Funct. Mater.* 25 (2015) 4985-4993.
- [34] Y. Gang, X.L. C, K.J. Wang, X.F. Wang, H.P. Sun, Y.G. Chen. Experimental study on

- interfacial reaction of CNTs/Al matrix composites. *Mining and Metallurgical Engineering* 33(1) (2013) 109-112.
- [35] D. Dutta, S. Chandra, A. K. Swain, D. Bahadur. SnO₂ Quantum Dots-Reduced Graphene Oxide Composite for Enzyme-Free Ultrasensitive Electrochemical Detection of Urea. *Anal. Chem.* 86 (2014) 5914–5921.
- [36] Z.Y. Yu, Z.Q. Tan, R. Xu, G. Ji, G.L. Fan, D.B. Xiong, Q. Guo, Z.Q. Li, D. Zhang. Enhanced load transfer by designing mechanical interfacial bonding in carbon nanotube reinforced aluminum composites. *Carbon* 146 (2019) 155-161.
- [37] R.P. Messner, Y.M. Chiang. Processing of reaction-bonded silicon carbide without residual silicon phase. *Cera Engi and Sci Proc.* 9(7~ 8) (1988) 1053-1059.
- [38] B. R. Pamplin. *Crystal Growth*. Pergamon Press. 1980: 58~60.
- [39] X.F. Du, T. Gao, D.K. Li, Y.Y. Wu, X.F. Liu. A novel approach to synthesize SiC particles by in situ reaction in Al-Si-C alloys. *J. Alloy. Compd.* 588 (2014) 374-377.
- [40] Z.Y. Xiu, W.S. Yang, R.H. Dong, M. Hussain, L.T. Jiang, Y.X. Liu, G.H. Wu. Microstructure and Mechanical Properties of 45 vol.% SiCp/7075Al Composite. *J. Mater. Sci. Technol.* 31 (2015) 930-934.
- [41] Y. Sun, H. Cui, L. Gong, J. Chen, P. Shen, C. Wang. Field nanoemitter: onedimension Al₄C₃ ceramics. *Nanoscale* 3(7) (2011) 2978-82.
- [42] S.F. Li, K. Kondoh, H. Imai, B. Chen, L. Jia, J. Umeda, Y.B. Fu. Strengthening behavior of in situ-synthesized (TiC-TiB)/Ti composites by powder metallurgy and hot extrusion. *Mater. & Design* 95 (2016) 127-32.
- [43] B. Chen, S. Li, H. Imai, L. Jia, J. Umeda, M. Takahashi, K. Kondoh. Load transfer strengthening in carbon nanotubes reinforced metal matrix composites via in situ tensile

- tests. *Compo. Sci. Technol.* 113 (2015) 1-8.
- [44] A. Slipenyuk, V. Kuprin, Yu. Milman, V. Goncharuk, J. Eckert. Properties of P/M processed particle reinforced metal matrix composites specified by reinforcement concentration and matrix-to-reinforcement particle size ratio. *Acta Mater.* 54 (2006) 157-166.
- [45] Z. Zhang, D.L. Chen. Consideration of Orowan strengthening effect in particulate-reinforced metal matrix nanocomposites: a model for predicting their yield strength. *Scr. Mater.* 54 (2006) 1321-1326.
- [46] Lloyd D J. Particle reinforced aluminium and magnesium matrix composites. *Metal. Rev.* 39(1)(1994) 1-23.
- [47] M. Geni, M. Kikuchi. Damage analysis of aluminum matrix composite considering non-uniform distribution of SiC particles. *Mechanics & Engineering* 46(9)(2002) 3125-3133.
- [48] X. Zhang, S.F. Li, B. Pan, D. Pan, S.Y. Zhou, S.H. Yang, L. Jia, K. Kondoh. A novel strengthening effect of in-situ nano Al_2O_3 on CNTs reinforced aluminum matrix nanocomposites and the matched strengthening mechanisms. *J. Alloy. Compd.* 764 (2018) 279-288.
- [49] Z.W. Cui, J.J. Liu, C.C. Wang, D. Liang. The synergy of carbon nanotubes and alumina particles in copper matrix composites. *Powder Metall. Technol.* 32(5) (2014) 346-351.
- [50] J. Hashim, L. Looney, M.S.J. Hashmi. The wettability of SiC particles by molten aluminium alloy. *J. Mater. Process Technol.* 119 (2001) 324.
- [51] K. Landry, N. Eustathopoulos. Dynamics of wetting in reactive metal/ceramic system: linear spreading. *Acta Mater.* 44(10)(1996) 3923-3932.
- [52] T. Young. An essay on the cohesion of fluids. *Philosophical Transactions of the Royal Society of London* 95 (1805) 65-87.

- [53] B.J. Keene. Review of data for the surface tension of pure metals. *Int. Mater. Rev.* 38 (1993) 157.
- [54] Z.Y. Liu, B.L. Xiao, W.G. Wang, Z.Y. Ma. Tensile strength and electrical conductivity of carbon nanotube reinforced aluminum matrix composites fabricated by powder metallurgy combined with friction stir processing. *J. Mater. Sci. Technol.* 30(7) (2014) 649-655.
- [55] D.H. Nam, S.I. Cha, B.K. Lim, H.M. Park, D.S. Han, S.H. Hong. Synergistic strengthening by load transfer mechanism and grain refinement of CNT/Al–Cu composites. *Carbon* 50 (2012) 2417-2423.
- [56] R. George, K.T. Kashyap, R. Rahul, S. Yamdagni. Strengthening in carbon nanotube/aluminium (CNT/Al) composites. *Scr. Mater.* 53 (2005) 1159-1163.
- [57] W. Zhou, T. Yamaguchi, K. Kikuchi, N. Nomura, A. Kawasaki, Effectively enhanced load transfer by interfacial reactions in multi-walled carbon nanotube reinforced Al matrix composites. *Acta Mater.* 125 (2017) 369-376.
- [58] B. Chen, J. Shen, X. Ye, L. Jia, S. Li, K. Kondon. Length effect of carbon nanotubes on the strengthening mechanisms in metal matrix composites. *Acta Mater.* 140 (2017) 317-325.